

Mechanical pressure and work cycle of confined active Brownian particles

Paolo Malgaretti,^{1,2,*} Piotr Nowakowski,^{1,2} and Holger Stark³

¹Max-Planck-Institut für Intelligente Systeme, Heisenbergstr. 3, D-70569 Stuttgart, Germany

²IV. Institut für Theoretische Physik, Universität Stuttgart, Pfaffenwaldring 57, D-70569 Stuttgart, Germany

³Institut für Theoretische Physik, Technische Universität Berlin, Hardenbergstrasse 36, 10623 Berlin, Germany

We derive an analytic expression for the mechanical pressure of a generic one-dimensional model of confined active Brownian particles (ABPs) that is valid for all values of Péclet number Pe and all confining scenarios. Our model reproduces the known scaling of bulk pressure with Pe^2 while in strong confinement pressure scales with Pe . Our analytic results are very well reproduced by simulations of ABPs in 2D. We use the pressure formula to calculate both the work performed by an active engine and its efficiency. In particular, efficiency is maximized for work cycles with finite period and not in the limit of infinitely slow cycles as in thermodynamic engines.

The properties and structure formation of active systems are quite different as compared to their equilibrium counterparts [1–7]. This becomes particularly apparent in confinement [8–17]. Indeed, active particles accumulate at walls [18], interfaces [19, 20], as well as obstacles [21, 22], and in denser suspensions they show motility-induced phase separation [23]. One of the key macroscopic quantities of interest is the mechanical pressure Π that active particles exert on confining walls [10, 24–26]. Such a quantity is crucial for determining the performance of devices rectifying active motion [27–29], for work cycles that exploit active baths [30], for invasion of active particles into confining space [31], as well as evaporation [32] and wetting [33] in active fluids.

Predicting the value of Π for active systems is not trivial since, due to the active nature of the particles, pressure is, in general, no longer a thermodynamic state function [34]. It is not even an intensive variable since it depends explicitly on extensive variables (like number of particles), as we show below. Several articles [10, 24, 25] have reported independently the characteristic scaling for the pressure, $\Pi \propto Pe^2$, where the Péclet number $Pe = v_{\text{act}}R/D$ depends on the active velocity v_{act} , the linear size R , and the diffusion coefficient D of the particle. This relation for pressure has been derived for semi-infinite systems. However, the dynamics of active Brownian particles (ABPs) is very sensitive to the presence of boundaries [8–16] and it is not obvious that the scaling for the pressure also holds for *confined* ABPs. Indeed, recent numerical works [9, 10] have shown that the pressure of strongly confined active particles scales as $\Pi \propto Pe$. Therefore, the scaling of Π with Pe depends on the system size. At the moment, a comprehensive relation, valid for all confining scenarios, between the pressure and the microscopic parameters (such as active velocity and tumbling rate), which control the dynamics of ABPs, is still lacking.

In this letter we derive a closed-form expression for the pressure exerted by confined ABPs that is valid for all values of Pe and all confining scenarios. In order to do so, we consider simple ABPs that only move in one dimension either along the x axis (“up” state) or

against it (“down” state) and that tumble between both states. Furthermore, the ABPs experience a confining soft potential such that, in the limit of diverging potential strength, our model retrieves the case of ABPs confined in a box with hard walls. In this standard case, the calculated mechanical pressure displays multiple scalings with Pe . In particular, when particles undergo multiple tumbling events between subsequent collisions with the walls (diffusive regime), pressure scales as $\Pi \propto Pe^2$ in agreement with Refs. [10, 24, 34]. In contrast, for strongly confined active colloids or for very large values of Pe (as the one attained for dry macroscopic active matter [35–40]) particles only undergo a few (if at all) tumbling events (ballistic regime) and the pressure scales as $\Pi \propto Pe$. Our analytic predictions for the pressure are in very good agreement with results from numerical simulations of ABPs in two dimensions and with the numerical results of Refs. [9, 10]. Thus, despite its simplicity our model captures the essence of the dynamics of confined ABPs. Hence, it can be used to predict the mechanical pressure of ABPs on both the microscopic ($\sim \mu\text{m}$) and macroscopic ($\sim \text{cm}, \text{m}$) scale in all confining scenarios.

We apply the analytical formula for the mechanical pressure to the recently introduced work cycle of active engines [30]; devices that exploit the capability of a bath of ABPs to perform directed work. We find that the work is governed by two unitless parameters and that the efficiency of quasistatic work cycles is optimal for a finite period in contrast to thermodynamic engines.

Model The N noninteracting ABPs experience the confining potential

$$\beta U(z) = \begin{cases} f(z/L - 1) & z > L, \\ 0 & -L \leq z \leq L, \\ -f(z/L + 1) & z < -L, \end{cases} \quad (1)$$

where L is the size of the system (not including the soft walls), f controls the softness of the walls, $\beta = 1/(k_B T)$, k_B is the Boltzmann constant, and T is the temperature. Within the overdamped regime, the time evolution of the reduced densities for “up” (ρ_{\uparrow}) and “down” (ρ_{\downarrow}) states, which we express as functions of the dimension-

less position $x = z/L$ and with time in units of L^2/D , are governed by

$$\dot{\rho}_{\uparrow}(x) = -\partial_x J_{\uparrow} - \Gamma \frac{L^2}{R^2} [\rho_{\uparrow}(x) - \rho_{\downarrow}(x)], \quad (2a)$$

$$\dot{\rho}_{\downarrow}(x) = -\partial_x J_{\downarrow} + \Gamma \frac{L^2}{R^2} [\rho_{\uparrow}(x) - \rho_{\downarrow}(x)]. \quad (2b)$$

(For simplicity we do not denote explicitly the dependence on time.) In Eqs. (3) we have identified the fluxes as

$$J_{\uparrow}(x) = -\left[\partial_x \rho_{\uparrow}(x) - \frac{L}{R} \text{Pe} \rho_{\uparrow}(x) + \rho_{\uparrow}(x) \beta \partial_x U(x)\right], \quad (3a)$$

$$J_{\downarrow}(x) = -\left[\partial_x \rho_{\downarrow}(x) + \frac{L}{R} \text{Pe} \rho_{\downarrow}(x) + \rho_{\downarrow}(x) \beta \partial_x U(x)\right], \quad (3b)$$

and we have introduced

$$\text{Pe} = v_{\text{act}} R/D, \quad \Gamma = \gamma R^2/D, \quad (4)$$

the particle Péclet number Pe and dimensionless tumbling rate Γ defined as tumbling rate γ times the diffusion time scale R^2/D . For later use, we note that $\text{Pe}^2/\Gamma = v_{\text{act}}^2 \gamma^{-1}/D$ is the ratio of active to passive diffusion coefficients.

By solving Eqs. (2) in steady state using piecewise solutions in the three regions of $\beta U(x)$ (see suppl. mat.), we compute the unitless mechanical pressure exerted on the right wall (the same results hold for the left wall),

$$\Pi = \int_1^{\infty} [\rho_{\uparrow}(x) + \rho_{\downarrow}(x)] f dx. \quad (5)$$

Pressure In order to study the case of ABPs confined within a box, we take the limit of the hard-core potential ($f \rightarrow \infty$, see suppl. mat.). In this limit, Π becomes

$$\Pi_{\infty} = \bar{\rho} \frac{R^2}{L^2} \frac{\kappa_c^3 \cosh \kappa_c}{\text{Pe}^2 \sinh \kappa_c + 2\Gamma \kappa_c \cosh \kappa_c}. \quad (6)$$

Here, $\bar{\rho} = NR/2L$ is the unitless number density and

$$\kappa_c = \kappa L = \frac{\sqrt{\text{Pe}^2 + 2\Gamma}}{R} L, \quad (7)$$

where κ is the inverse of the effective length that characterizes the exponential decay of the density profile close to the wall [47]. We remark that κ depends solely on microscopic parameters and not on the system size. In particular, when $\kappa_c \gg 1$, Eq. (6) is approximated by

$$\Pi_{\infty} \simeq \bar{\rho} \frac{R^2}{L^2} \frac{\kappa_c^3}{\text{Pe}^2 + 2\Gamma \kappa_c}. \quad (8)$$

The regime $\kappa_c \gg 1$ is typical for active matter as it occurs whenever either $\text{Pe} \gg R/L$ or $\Gamma \gg R^2/L^2$. The latter means that during passive diffusion across the system, tumbling occurs frequently. Therefore, in the following we focus on the relevant case of $\kappa_c \gg 1$.

Figures 1(a) and (b) show that Π_{∞} grows monotonically upon increasing Pe , as expected. In the limit of small Péclet numbers, $\text{Pe} \ll \text{Pe}_{\text{small}} = \sqrt{2\Gamma}$, Eq. (8) gives

$$\Pi_{\infty}^{\text{small}} \simeq \bar{\rho} \left(1 + \frac{\text{Pe}^2}{2\Gamma}\right). \quad (9)$$

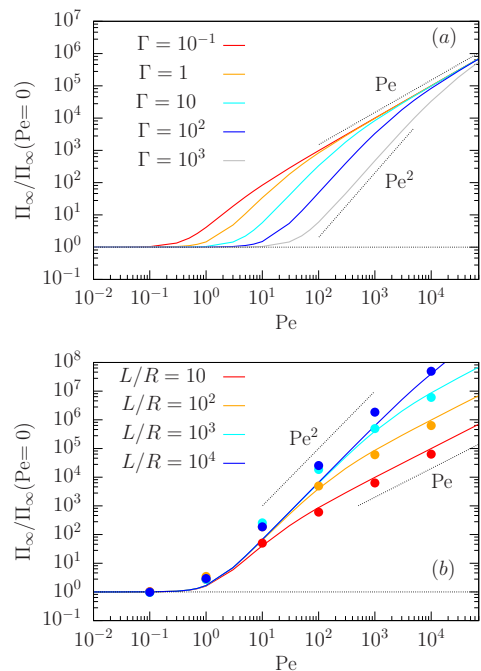


FIG. 1: (a): Pressure Π_{∞} as function of Pe for diverse values of Γ and $L = 10R$. (b): Π_{∞} as function of Pe for $\Gamma = 3/4$ and diverse values of L/R . The dots present the results of 2D numerical simulations of ABPs with no fitting parameters.

Thus, for vanishingly small Pe , Π_{∞} reduces to its equilibrium value $\Pi_{\infty}^0 = \bar{\rho}$. We remark that Π_{∞}^0 does not depend explicitly on system size L or particle number N , as required for an intensive thermodynamic quantity. For $\text{Pe} \simeq \text{Pe}_{\text{small}}$, activity starts to dominate the pressure. Using Eqs. (4), the condition $\text{Pe} \simeq \text{Pe}_{\text{small}}$ implies $D_{\text{act}} = v_{\text{act}}^2/\gamma \simeq D$. Thus, the pressure starts to grow with Pe^2 when the active contribution to the total diffusion coefficient $D_{\text{eff}} = D + D_{\text{act}}$ becomes dominant [41].

For large Péclet numbers ($\text{Pe} \gg \text{Pe}_{\text{small}}$) we obtain from Eq. (8):

$$\Pi_{\infty}^{\text{large}} \simeq \bar{\rho} \frac{L}{R} \text{Pe} \left(1 + \frac{2\Gamma L}{\text{Pe} R}\right)^{-1}. \quad (10)$$

When $\text{Pe} \gg \text{Pe}_{\text{large}} = 2\Gamma L/R$, pressure Π_{∞} attains its asymptotic form, $\Pi_{\infty} \simeq \bar{\rho} \text{Pe} L/R = N \text{Pe}/2$, growing linearly in Pe . In this regime Π_{∞} is no longer an intensive variable since it depends explicitly on particle number N .

The crossover between the different scalings of Π_{∞} with Pe occurs at $\text{Pe} = \text{Pe}_{\text{large}} = 2\Gamma L/R$ or when the ballistic time L/v_{act} is comparable to the mean run time $1/\gamma$ between two tumbling events. Thus, in the asymptotic regime where $L/v_{\text{act}} \ll 1/\gamma$, particles only undergo a few (if at all) tumbling events between subsequent collisions with the walls (ballistic regime). As a result, they spend the large amount of time at the boundaries. Therefore, the pressure increases linearly with Pe and depends explicitly only on particle number and not on system size.

In the opposite case $L/v_{\text{act}} \gg 1/\gamma$ (*i.e.*, $\text{Pe} \ll \text{Pe}_{\text{large}}$), the particles undergo multiple tumbling events between subsequent collisions with the walls (diffusive regime). In this regime, increasing Pe has a twofold effect: first, it directly enhances pressure when the particles hit the wall, and second, it reduces the number of tumbling events between to subsequent collisions at the walls and thereby enhances the density of the particles at the wall. This twofold effect explains the quadratic dependence of Π_{∞} on Pe , as shown in both panels of Fig. 1.

Accordingly, Fig.1(a) shows that the scaling of the pressure with Pe changes dramatically upon changing the tumbling rate Γ . At the micrometric scale, this result is crucial for confined bacterial suspensions [42, 43], whose tumbling rate depends on both the biology of the bacteria as well as on external control parameters [48]. At the macroscopic scale our result is crucial for determining the pressure of dry active matter, such as small robots [36], ants [37, 38], sheep [39], and humans [35, 40], just to mention a few among others.

For active colloids, such as Janus particles, Γ is controlled by the rotational diffusion coefficient D_{rot} , which depends on their size and shape. For spherical particles $D_{\text{rot}} = \frac{3}{4} \frac{D}{R^2}$, which in 2D equals γ so that $\Gamma = 3/4$. For this case, Fig. 1(b) presents Π_{∞} versus Pe for diverse system sizes. Interestingly, for typical values of the Péclet number ($\text{Pe} \simeq 1 - 100$) and system sizes ($L \gtrsim 100R$) that have been investigated experimentally [44] or numerically [45], our model predicts $\Pi_{\infty} \propto \text{Pe}^2$, in agreement with Ref. [10, 24, 25, 34, 45, 46]. However, for smaller system sizes $L \simeq 10R$ or for very large values of the Péclet number, $\text{Pe} \gg \text{Pe}_{\text{large}}$, the asymptotic behavior $\Pi_{\infty} \propto \text{Pe}$ is retrieved.

In order to check the validity of our expression against more realistic models, we performed 2D simulations of spherical ABPs characterized by $\Gamma = 3/4$, where the particle orientations diffused on the unit circle (see suppl. mat. for more details on the simulations). The results are included in Fig. 1(b). Interestingly, without using any fitting parameters, the agreement between the theoretical predictions and the results of the numerical simulations is very good for all values of Pe and L that we tested. Hence, our simple two-state model captures the essence of the dynamics of confined ABPs.

Compressibility Having an explicit expression for the pressure [cf. Eq. (6)], we can calculate explicitly the unitless compressibility $H_{\infty} = -(\partial\Pi_{\infty}/\partial L)^{-1}/L$ (see suppl. mat.). For the relevant case of $\kappa_c \gg 1$, it reduces to

$$H_{\infty} \simeq \frac{1}{\Pi_{\infty}} \left(1 + \frac{\text{Pe}^2}{2\Gamma\kappa_c} \right) \quad (11)$$

Besides the $1/\Pi_{\infty}$ term of an ideal gas, H_{∞} additionally depends on Pe , Γ , and κ_c . In particular, we recall that κ_c grows with system size L . This is in contrast to equilibrium systems, where the compressibility as an

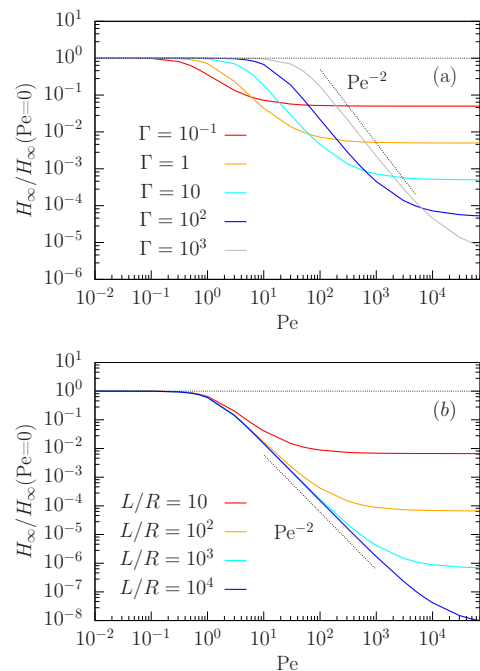


FIG. 2: (a): Compressibility H_{∞} as function of Pe for diverse values of Γ and for $L/R = 10$. (b): H_{∞} as function of Pe for diverse values of L/R and for $\Gamma = 3/4$.

intensive quantity solely depends on intensive variables, such as pressure, temperature, and chemical potential and not on system size. Figure 2(a) shows H_{∞} plotted versus Pe for $L = 10R$ and diverse values of Γ . Similar to the behavior of pressure, upon increasing Pe beyond $\text{Pe}_{\text{small}} = \sqrt{2\Gamma}$, the compressibility starts to decrease as Pe^{-2} due to the prefactor $1/\Pi_{\infty}$ [cf. Eq. (9)] and then, beyond $\text{Pe} \simeq \text{Pe}_{\text{large}} = 2\Gamma L/R$, it reaches the normalized plateau value $R^2/(L^2 2\Gamma)$. In particular, larger values of Γ delay the onset of the decrease of H_{∞} and they also lower the plateau value since more tumbling releases pressure generated by the active particles. Figure 2(b) shows the relevant case of active colloids and that not only pressure Π_{∞} but also H_{∞} retains a dependence on the system size.

Active Engine We can exploit the exact expression for the pressure to calculate the work performed by the system during the periodic work cycle shown in Fig. 3(a). Work is performed by the system only when there is a change in the system size $2L$. Assuming that these changes are sufficiently slow so that the mechanical pressure can adjust instantaneously, the total dimensionless work per particle along a cycle reads:

$$W = \int_{L_1}^{L_2} \frac{\Pi_{\infty}(L, \text{Pe}_2)}{N/2} \frac{dL}{R} - \int_{L_1}^{L_2} \frac{\Pi_{\infty}(L, \text{Pe}_1)}{N/2} \frac{dL}{R}, \quad (12)$$

where $N/2$ is the number of particles in L . Figure 3(b) shows that for small system sizes the work performed by the system grows linearly with L_1 (for fixed ratio L_2/L_1). In this regime the work is insensitive to Γ [blue and cyan

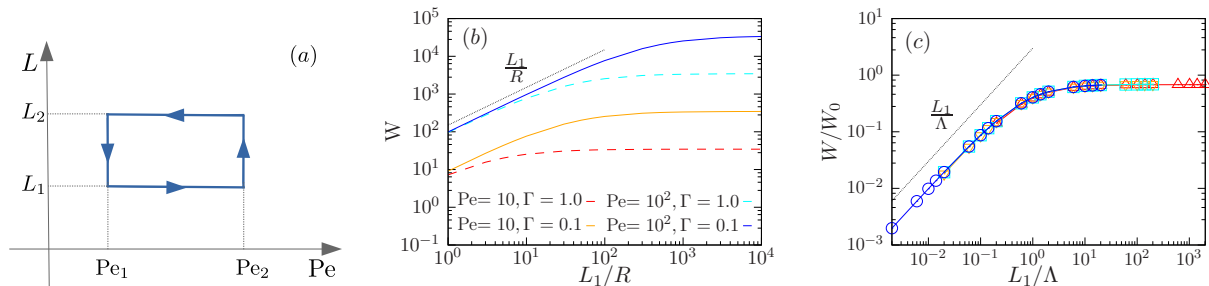


FIG. 3: a): Scheme of the work cycle of the active engine in the Pe - L plane. b) Work W performed by one cycle of the active engine as function of L_1 with $L_2 = 2L_1$ and $Pe_1 = 0$ for diverse values of $Pe_2 = Pe$ and Γ . c) Rescaled data of panel (b)

curves as well as red and orange curves lie on top of each other in Fig. 3(b)], while the overall amount of work depends on Pe . Upon increasing L_1 further, the work W reaches a plateau. Here, W increases upon decreasing Γ for both values of Pe , since tumbling reduces the pressure of the expanding system. The dependence of W on Γ is remarkable since it shows that the work performed by the active system explicitly depends on the tumbling rate, *i.e.*, on some microscopic time scale. Such a dependence does not occur in passive systems and therefore is a signature of the active nature of the system under study. In contrast, the dependence of W on Pe is clear since the active motion of the ABPs generates the force with which they push against the wall.

All these observations can be rationalized by considering the limit $\kappa_c \gg 1$ in Eq. (12) which gives

$$W \simeq W_0 \ln \left[\frac{1 + L_2/\Lambda}{1 + L_1/\Lambda} \right] - \ln \left[\frac{L_2}{L_1} \right]. \quad (13)$$

Here, we have identified the effective length Λ and strength W_0 of the work cycle,

$$\Lambda = \frac{Pe^2 R}{2\Gamma\sqrt{Pe^2 + 2\Gamma}}, \quad W_0 = 1 + \frac{Pe^2}{2\Gamma}. \quad (14)$$

After rescaling work by W_0 and system size by Λ , for $W_0 \gg 1$ all curves from Fig. 3(b) collapse onto one master curve, as demonstrated in Fig. 3(c). In the regime $Pe \gg Pe_{\text{small}} = \sqrt{2\Gamma}$ the parameters become

$$\Lambda \simeq \frac{v_{\text{act}}}{\gamma}, \quad W_0 \simeq \frac{v^2}{D\gamma} = \frac{D_{\text{act}}}{D}, \quad (15)$$

i.e., the threshold length Λ is the typical distance travelled by the particle between two tumbling events, whereas the work strength W_0 is proportional to the ratio of active to passive diffusion coefficients. In particular, for large systems sizes, $L_1, L_2 \gg \Lambda$, we have

$$W \approx (W_0 - 1) \ln(L_2/L_1) \simeq W_0 \ln(L_2/L_1). \quad (16)$$

Thus, the work per particle over one cycle solely depends on W_0 and its dependence on system size is reminiscent of the work done by a passive ideal gas.

Efficiency Finally, we define the efficiency of the work cycle as the ratio of the work performed by the system, W , to the total energy injected into the system,

$$\eta = W / (W + W_{\text{irr}}), \quad (17)$$

where W_{irr} accounts for the energy spent in dissipative processes. In particular, W_{irr} is the sum of two contributions. First, we express the power dissipated by the particles due to their active motion as $W_{\text{irr}}^{\text{pcl}} = N\mathcal{P}\tau$, where \mathcal{P} is the mean power dissipated by a single particle during one work cycle of period τ . Second, compression and expansion of the system contribute to dissipation. Assuming instantaneous changes of Pe , the velocity is $2(L_2 - L_1)/\tau = 2\Delta L/\tau$ and the total dissipated energy becomes $W_{\text{irr}}^{\text{sys}} = 4W\Delta L^2/\tau$, where W plays the role of an effective friction coefficient. All in all we obtain

$$W_{\text{irr}} = W_{\text{irr}}^{\text{pcl}} + W_{\text{irr}}^{\text{sys}} = N\mathcal{P}\tau + 4W\Delta L^2/\tau. \quad (18)$$

Maximizing the efficiency with respect to τ amounts to minimizing W_{irr} which gives $\tau = (4W\Delta L^2/N\mathcal{P})^{1/2}$. Accordingly, even for quasi-static expansions η is maximized for a *finite* cycle time τ in stark contrast to the quasi-static limit $\tau \rightarrow \infty$ of thermodynamic engines.

Conclusions Based on a one-dimensional model for run-and-tumble particles, we have derived an analytic expression for the mechanical pressure ABPs exert on bounding walls. In the limit of large systems we reproduce the well-known scaling of the bulk pressure with Pe^2 . In contrast, for either strongly confined micrometric ABPs or macroscopic ABPs with very large Pe , the pressure scales with Pe and is no longer an intensive variable. We clearly rationalize the regimes where the different scalings are observed. Furthermore, two-dimensional Brownian dynamics simulations of ABPs quantitatively agree with our analytic expression and thereby show its generality.

Our analytic formula for pressure allows to systematically explore basic features of confined active systems between bulk- and surface-driven behavior. For the recently introduced active engines we have calculated the work performed during one cycle in the quasi-static limit. It explicitly depends on the characteristic time scale Γ^{-1} ,

a feature that is absent in conventional thermodynamic engines. Furthermore, the efficiency is maximized at a *finite* cycle rate due to the inherent dissipation, in clear contrast to thermodynamic engines where infinitely small rates avoid dissipation.

* Electronic address: malgaretti@is.mpg.de

- [1] S. Ramaswamy, *Annu. Rev. Condens. Matter Phys.* **1**, 323 (2010).
- [2] P. Romanczuk, M. Bär, W. Ebeling, B. Lindner, and L. Schimansky-Geier, *EPJST* **202**, 1 (2012).
- [3] M. Marchetti, J. Joanny, S. Ramaswamy, T. Liverpool, J. Prost, M. Rao, and R. A. Simha, *Rev. Mod. Phys.* **85**, 1143 (2013).
- [4] J. Elgeti, R. Winkler, and G. Gompper, *Rep. Prog. Phys.* **78**, 056601 (2015).
- [5] A. Zöttl and H. Stark, *Journal of Physics: Condensed Matter* **28**, 253001 (2016).
- [6] C. Bechinger, R. Di Leonardo, H. Löwen, C. Reichhardt, G. Volpe, and G. Volpe, *Rev. Mod. Phys.* **88**, 045006 (2016).
- [7] G. Gompper, R. G. Winkler, T. Speck, A. Solon, C. Nardin, F. Peruani, H. Löwen, R. Golestanian, U. B. Kaupp, L. Alvarez, et al., *Journal of Physics: Condensed Matter* **32**, 193001 (2020).
- [8] C. F. Lee, *New Journal of Physics* **15**, 055007 (2013).
- [9] X. Yang, M. L. Manning, and M. C. Marchetti, *Soft Matter* **10**, 6477 (2014).
- [10] B. Ezhilan, R. Alonso-Matilla, and D. Saintillan, *Journal of Fluid Mechanics* **781**, R4 (2015).
- [11] F. Ginot, I. Theurkauff, D. Levis, C. Ybert, L. Bocquet, L. Berthier, and C. Cottin-Bizonne, *Phys. Rev. X* **5**, 011004 (2015).
- [12] P. Malgaretti, M. N. Popescu, and S. Dietrich, *Soft Matter* **12**, 4007 (2016).
- [13] P. Malgaretti and H. Stark, *The Journal of Chemical Physics* **146**, 174901 (2017).
- [14] Y. Fily, A. Baskaran, and M. F. Hagan, *The European Physical Journal E* **40** (2017).
- [15] T. Ostapenko, F. J. Schwarzendahl, T. J. Böddeker, C. T. Kreis, J. Cammann, M. G. Mazza, and O. Bäümchen, *Phys. Rev. Lett.* **120**, 068002 (2018).
- [16] S. Das, G. Gompper, and R. G. Winkler, *New Journal of Physics* **20**, 015001 (2018).
- [17] T. Peter, P. Malgaretti, N. Rivas, A. Scagliarini, J. Harting, and S. Dietrich, *Soft Matter* **16**, 3536 (2020).
- [18] J. Elgeti and G. Gompper, *EPL (Europhysics Letters)* **101**, 48003 (2013).
- [19] J. Simmchen and P. Malgaretti, *ChemNanoMat* **3**, 790 (2017).
- [20] P. Malgaretti, M. N. Popescu, and S. Dietrich, *Soft Matter* **18**, 1375 (2018).
- [21] D. Takagi, J. Palacci, A. B. Braunschweig, M. J. Shelley, and J. Zhang, *Soft Matter* **10**, 1784 (2014).
- [22] M. Zeitz, K. Wolff, and H. Stark, *Eur. Phys. J. E* **40**, 23 (2017).
- [23] M. E. Cates and J. Tailleur, *Annual Review of Condensed Matter Physics* **6**, 219 (2015).
- [24] S. C. Takatori, W. Yan, and J. F. Brady, *Phys. Rev. Lett.* **113**, 028103 (2014).
- [25] A. P. Solon, J. Stenhammar, R. Wittkowski, M. Kardar, Y. Kafri, M. E. Cates, and J. Tailleur, *Phys. Rev. Lett.* **114**, 198301 (2015).
- [26] R. Wittmann, F. Smallenburg, and J. M. Brader, *J. Chem. Phys.* **150**, 174908 (2019).
- [27] A. Sokolov, M. M. Apodaca, B. A. Grzybowski, and I. S. Aranson, *Proc. Natl. Acad. Sci.* **107**, 969 (2010).
- [28] R. Di Leonardo, L. Angelani, D. Dell’Arciprete, G. Ruocco, V. Iebba, S. Schippa, M. P. Conte, F. Mecarini, F. De Angelis, and E. Di Fabrizio, *Proc. Natl. Acad. Sci.* **107**, 9541 (2010).
- [29] A. Kaiser, A. Peshkov, A. Sokolov, B. ten Hagen, H. Löwen, and I. S. Aranson, *Phys. Rev. Lett.* **112**, 158101 (2014).
- [30] T. Ekeh, M. E. Cates, and E. Fodor, *Phys. Rev. E* **102**, 010101 (2020).
- [31] F. Kempf, R. Mueller, E. Frey, J. M. Yeomans, and A. Doostmohammadi, *Soft Matter* **15**, 7538 (2019).
- [32] T. Andac, P. Weigmann, S. K. P. Velu, E. Pine, G. Volpe, G. Volpe, and A. Callegari, *Soft Matter* **15**, 1488 (2019).
- [33] N. Sepúlveda and R. Soto, *Phys. Rev. Lett.* **119**, 078001 (2017).
- [34] A. P. Solon, Y. Fily, A. Baskaran, M. E. Cates, Y. Kafri, M. Kardar, and J. Tailleur, *Nature Physics* **11**, 673 (2015).
- [35] M. Moussaad, M. Kapadia, T. Thrash, R. W. Sumner, M. Gross, D. Helbing, and C. Halscher, *Journal of The Royal Society Interface* **13**, 20160414 (2016).
- [36] M. Mijalkov, A. McDaniel, J. Wehr, and G. Volpe, *Phys. Rev. X* **6**, 011008 (2016).
- [37] C. Saloma, G. J. Perez, G. Tapang, M. Lim, and C. Palmes-Saloma, *Proc. Natl. Acad. Sci.* **100**, 11947 (2003).
- [38] E. Altshuler, O. Ramos, Y. Nuñez, J. Fernandez, A. Batista-Leyva, and C. Noda, *The American Naturalist* **166**, 643 (2005).
- [39] I. Zuriguel, J. Olivares, J. M. Pastor, C. Martín-Gómez, L. M. Ferrer, J. J. Ramos, and A. Garcimartín, *Phys. Rev. E* **94**, 032302 (2016).
- [40] I. Zuriguel, I. naki Echeverria, D. Maza, R. C. Hidalgo, C. Martín-Gomez, and A. Garcimartin, *Safety Science* **121**, 394 (2020).
- [41] J. R. Howse, R. A. L. Jones, A. J. Ryan, T. Gough, R. Vafabakhsh, and R. Golestanian, *Phys. Rev. Lett.* **99**, 048102 (2007).
- [42] J. Najafi, M. R. Shaebani, T. John, F. Altegoer, G. Bange, and C. Wagner, *Science Advances* **4** (2018).
- [43] M. Seyrich, Z. Alirezaeizanjani, C. Beta, and H. Stark, *New. J. Phys.* **20**, 103033 (2018).
- [44] G. Junot, G. Briand, R. Ledesma-Alonso, and O. Dautot, *Phys. Rev. Lett.* **119**, 028002 (2017).
- [45] R. G. Winkler, A. Wysocki, and G. Gompper, *Soft Matter* **11**, 6680 (2015).
- [46] L. Caprini and U. Marini Bettolo Marconi, *Soft Matter* **14**, 9044 (2018).
- [47] The exponential decay and the associated decay length (Eq.(7)) are valid for all values of Pe and L . In particular, for small values of Pe Eq. (7) reduces to $\kappa \simeq \Gamma$ in agreement with Ref. [18].
- [48] Typically, $\Gamma \gtrsim 100$ [42]. Even upon genetically switching off tumbling, the lower bound is $\Gamma \simeq 1$ due to rotational diffusion. In addition, in chemical gradients Γ can vary by a factor of five [43].

Supplemental Material

Model

In this section we analyze the dynamics of N noninteracting active Brownian particles (ABPs) confined in $1D$ and suspended in an equilibrium thermal bath. The ABPs are characterized by an “internal state” that determines the preferred direction of motion. When the particles are in the “up” state, the active contribution v_{act} to the overall velocity points to the right (parallel to x axis), while in “down” state it points to the left (antiparallel to x axis). The particles can randomly hop between the two states with the rate γ . Additionally, we assume that the particles experience a confining potential

$$\beta U(z) = \begin{cases} f \frac{z-L}{L} & \text{for } z > L, \\ 0 & \text{for } -L \leq z \leq L, \\ -f \frac{z+L}{L} & \text{for } z < -L, \end{cases} \quad (19)$$

such that when the center of mass of a particle is not in the region $-L \leq z \leq L$ there is a constant force pushing the particle back into the region. The choice of a piecewise linear potential allows us for further analytical insight.

In the following, instead of the number density of particles $\tilde{\rho}(z)$, we use the dimensionless quantities which we get by rescaling the distance $x = z/L$ and by multiplying $\tilde{\rho}$ by the particle size R

$$\rho(x) = R\tilde{\rho}(z = xL). \quad (20)$$

The potential in rescaled variables is

$$\beta U(x) = \begin{cases} f(x-1) & \text{for } x > 1, \\ 0 & \text{for } -1 \leq x \leq 1, \\ -f(x+1) & \text{for } x < -1, \end{cases} \quad (21)$$

and the normalization condition is

$$\int_{-\infty}^{\infty} \tilde{\rho}(z) dz = N \quad \mapsto \quad \int_{-\infty}^{\infty} \rho(x) dx = N \frac{R}{L}. \quad (22)$$

The time evolution of the dimensionless probability distributions of particles in the “up state” $\rho_{\uparrow}(x)$ and “down state” $\rho_{\downarrow}(x)$ are governed by

$$\dot{\rho}_{\uparrow}(x) = -\partial_x J_{\uparrow} - \Gamma \frac{L^2}{R^2} [\rho_{\uparrow}(x) - \rho_{\downarrow}(x)], \quad (23a)$$

$$\dot{\rho}_{\downarrow}(x) = -\partial_x J_{\downarrow} + \Gamma \frac{L^2}{R^2} [\rho_{\uparrow}(x) - \rho_{\downarrow}(x)], \quad (23b)$$

where we have used the dimensionless time, measured in L^2/D units. We have identified the fluxes as

$$J_{\uparrow}(x) = - \left[\partial_x \rho_{\uparrow}(x) - \frac{L}{R} \text{Pe} \rho_{\uparrow}(x) + \rho_{\uparrow}(x) \beta \nabla U(x) \right], \quad (24a)$$

$$J_{\downarrow}(x) = - \left[\partial_x \rho_{\downarrow}(x) + \frac{L}{R} \text{Pe} \rho_{\downarrow}(x) + \rho_{\downarrow}(x) \beta \nabla U(x) \right], \quad (24b)$$

with

$$\text{Pe} = \frac{v_{\text{act}} R}{D}, \quad \Gamma = \frac{\gamma R^2}{D}. \quad (25)$$

By introducing the total (dimensionless) density $\rho(x)$ and the density difference $\delta\rho(x)$

$$\rho(x) = \rho_{\uparrow}(x) + \rho_{\downarrow}(x), \quad \delta\rho(x) = \rho_{\uparrow}(x) - \rho_{\downarrow}(x), \quad (26)$$

we can rewrite Eqs. (23) as

$$\dot{\rho}(x) = -\partial_x J_\rho(x), \quad (27a)$$

$$\dot{\delta\rho}(x) = -\partial_x J_{\delta\rho}(x) - 2\Gamma \frac{L^2}{R^2} \delta\rho(x), \quad (27b)$$

with

$$J_\rho(x) = -\partial_x \rho(x) + \frac{L}{R} \text{Pe} \delta\rho(x) - \rho(x) \beta \partial_x U(x), \quad (28a)$$

$$J_{\delta\rho}(x) = -\partial_x \delta\rho(x) + \frac{L}{R} \text{Pe} \rho(x) - \delta\rho(x) \beta \partial_x U(x). \quad (28b)$$

We assume that there are no particles away from the box

$$\rho(x = \pm\infty) = 0, \quad \delta\rho(x = \pm\infty) = 0, \quad (29)$$

which additionally implies that for $x = \pm\infty$ there are no fluxes. In the steady state ($\dot{\rho}(x) = \dot{\delta\rho}(x) = 0$) Eqs. (27a) and (28a) gives

$$\delta\rho(x) = \frac{1}{\text{Pe}} \frac{R}{L} [\partial_x \rho(x) + \rho(x) \beta \partial_x U(x)]. \quad (30)$$

Substituting the above expression in Eq. (27b), using Eq. (28b), after some algebra we get the general equation

$$\begin{aligned} \partial_x^3 \rho + 2(\partial_x^2 \rho) \beta \partial_x U + (\partial_x \rho) \left(3\beta \partial_x^2 U - \frac{L^2}{R^2} \text{Pe}^2 + (\beta \partial_x U)^2 - 2\Gamma \frac{L^2}{R^2} \right) \\ + \rho \left(\beta \partial_x^3 U + 2(\beta \partial_x U) \beta \partial_x^2 U - 2\Gamma \frac{L^2}{R^2} \beta \partial_x U \right) = 0. \end{aligned} \quad (31)$$

For $-1 < x < 1$, where $U(x) = 0$, Eq. (31) simplifies to

$$\partial_x^3 \rho_c - (\partial_x \rho_c) (\text{Pe}^2 + 2\Gamma) \frac{L^2}{R^2} = 0, \quad (32)$$

Since we require $\rho(x)$ to have the symmetry $x \mapsto -x$, the solution of the above equation is

$$\rho_c(x) = A_c \cosh(\kappa_c x) + B_c, \quad \kappa_c^2 = (\text{Pe}^2 + 2\Gamma) \frac{L^2}{R^2}, \quad (33)$$

where A_c and B_c are, yet to be determined, constants.

For $x > 1$, where $\beta \partial_x U = f$, Eq. (31) takes the form

$$\partial_x^3 \rho_r + 2f(\partial_x^2 \rho_r) + \left(f^2 - \frac{L^2}{R^2} \text{Pe}^2 - 2\Gamma \frac{L^2}{R^2} \right) \partial_x \rho_r - 2\Gamma \frac{L^2}{R^2} f \rho_r = 0, \quad (34)$$

and the solution is

$$\rho_r(x) = A_1 e^{\kappa_1 x} + A_2 e^{\kappa_2 x} + A_3 e^{\kappa_3 x}, \quad (35)$$

where A_1, A_2 and A_3 are constants, and $\kappa_1 \geq \kappa_2 \geq \kappa_3$ are the roots of the polynomial

$$\mathcal{Q}(\kappa) = \kappa^3 + 2f\kappa^2 + \kappa \left(f^2 - \frac{L^2}{R^2} \text{Pe}^2 - 2\Gamma \frac{L^2}{R^2} \right) - 2\Gamma \frac{L^2}{R^2} f. \quad (36)$$

Since $\mathcal{Q}(0) = -2\Gamma \frac{L^2}{R^2} f < 0$ and $\mathcal{Q}(-f) = f \frac{L^2}{R^2} \text{Pe}^2 > 0$, the above polynomial has three different, real roots; κ_1 is positive and $\kappa_2, \kappa_3 < 0$. Using the Cardano's formula, after some algebra, we get

$$\kappa_1 = -\frac{2f}{3} + \frac{2}{3} \sqrt{f^2 + 3 \frac{L^2}{R^2} (2\Gamma + \text{Pe}^2)} \cos \frac{\theta}{3}, \quad (37a)$$

$$\kappa_2 = -\frac{2f}{3} + \frac{1}{3} \sqrt{f^2 + 3 \frac{L^2}{R^2} (2\Gamma + \text{Pe}^2)} \left(\sqrt{3} \sin \frac{\theta}{3} - \cos \frac{\theta}{3} \right), \quad (37b)$$

$$\kappa_3 = -\frac{2f}{3} + \frac{1}{3} \sqrt{f^2 + 3 \frac{L^2}{R^2} (2\Gamma + \text{Pe}^2)} \left(\sqrt{3} \sin \frac{\theta}{3} + \cos \frac{\theta}{3} \right), \quad (37c)$$

where the angle θ is given by

$$\sin \theta = \frac{\left[\left(f^2 + 3 \frac{L^2}{R^2} (2\Gamma + \text{Pe}^2) \right)^3 - \left(f^3 + 9f \frac{L^2}{R^2} (\Gamma - \text{Pe}^2) \right)^2 \right]^{1/2}}{\left[f^2 + 3 \frac{L^2}{R^2} (\text{Pe}^2 + 2\Gamma) \right]^{3/2}}, \quad \cos \theta = \frac{f^3 + 9f \frac{L^2}{R^2} (\Gamma - \text{Pe}^2)}{\left[f^2 + 3 \frac{L^2}{R^2} (\text{Pe}^2 + 2\Gamma) \right]^{3/2}}. \quad (38)$$

Due to the symmetry $x \mapsto -x$ there is no need to separately consider the case of $x < -1$.

In order to determine the integration constants we first impose the normalization condition (see Eq. (22))

$$\bar{\rho} = \frac{NR}{2L} = \int_0^\infty \rho(x) dx = \frac{A_c}{\kappa_c} \sinh \kappa_c + B_c + \frac{A_1}{\kappa_1} e^{\kappa_1 x} \Big|_1^\infty + \frac{A_2}{\kappa_2} e^{\kappa_2 x} \Big|_1^\infty + \frac{A_3}{\kappa_3} e^{\kappa_3 x} \Big|_1^\infty. \quad (39)$$

Since $\kappa_1 > 0$, the only way to satisfy the above condition is to require $A_1 = 0$. The resulting relation is

$$\bar{\rho} = \frac{A_c}{\kappa_c} \sinh \kappa_c + B_c - \frac{A_2}{\kappa_2} e^{\kappa_2} - \frac{A_3}{\kappa_3} e^{\kappa_3}. \quad (40a)$$

Three more relations come from the requirement that ρ , $\delta\rho$, J_ρ , and $J_{\delta\rho}$ are continuous at $x = 1$ (discontinuity of probability would lead to an infinite flux). The requirement of continuity of ρ gives

$$A_c \cosh \kappa_c + B_c = A_2 e^{\kappa_2} + A_3 e^{\kappa_3}, \quad (40b)$$

the continuity of $\delta\rho$ gives

$$A_c \kappa_c \sinh \kappa_c = A_2 \kappa_2 e^{\kappa_2} + A_3 \kappa_3 e^{\kappa_3} + f (A_2 e^{\kappa_2} + A_3 e^{\kappa_3}), \quad (40c)$$

and the continuity of $J_{\delta\rho}$ gives (we have used Eq. (40b) to simplify the formula)

$$A_c \kappa_c^2 \cosh \kappa_c = A_2 \kappa_2^2 e^{\kappa_2} + A_3 \kappa_3^2 e^{\kappa_3} + 2f (A_2 \kappa_2 e^{\kappa_2} + A_3 \kappa_3 e^{\kappa_3}) + f^2 (A_2 e^{\kappa_2} + A_3 e^{\kappa_3}). \quad (40d)$$

Since $J_\rho(x) = 0$, there is no equation coming from the requirement that J_ρ is continuous at $x = 1$. The solution of the linear Eqs. (40) is

$$A_c = -\bar{\rho} \frac{\kappa_2 \kappa_3 \kappa_c (f + \kappa_2) (f + \kappa_3)}{G_2 \cosh \kappa_c - G_1 \sinh \kappa_c}, \quad (41a)$$

$$B_c = \bar{\rho} \frac{\kappa_2 \kappa_3 \kappa_c \left[((f + \kappa_2) (f + \kappa_3) + \kappa_c^2) \cosh \kappa_c - (2f + \kappa_2 + \kappa_3) \kappa_c \sinh \kappa_c \right]}{G_2 \cosh \kappa_c - G_1 \sinh \kappa_c}, \quad (41b)$$

$$A_2 = \bar{\rho} \frac{e^{-\kappa_2} \kappa_2 \kappa_3 \kappa_c^2 (f + \kappa_3) [(f + \kappa_3) \sinh \kappa_c - \kappa_c \cosh \kappa_c]}{(\kappa_2 - \kappa_3) (G_2 \cosh \kappa_c - G_1 \sinh \kappa_c)}, \quad (41c)$$

$$A_3 = \bar{\rho} \frac{e^{-\kappa_3} \kappa_2 \kappa_3 \kappa_c^2 (f + \kappa_2) [(f + \kappa_2) \sinh \kappa_c - \kappa_c \cosh \kappa_c]}{(\kappa_3 - \kappa_2) (G_2 \cosh \kappa_c - G_1 \sinh \kappa_c)}, \quad (41d)$$

with

$$G_1 = \kappa_2 \kappa_3 (f + \kappa_2) (f + \kappa_3) - \kappa_c^2 \left[(f + \kappa_2)^2 - (\kappa_2 - 1) \kappa_3 (2f + \kappa_2) - (\kappa_2 - 1) \kappa_3^2 \right], \quad (41e)$$

$$G_2 = \kappa_2 \kappa_3 \kappa_c (f + \kappa_2) (f + \kappa_3) - \kappa_c^3 (f - \kappa_2 \kappa_3 + \kappa_2 + \kappa_3). \quad (41f)$$

Accordingly, the dimensionless mechanical pressure (measured in $k_B T/R$ units) of N noninteracting particles is

$$\begin{aligned} \Pi &= \int_1^\infty \beta \partial_x U(x) \rho(x) dx = \int_1^\infty f \rho(x) dx \\ &= \bar{\rho} f \kappa_c^2 \frac{\left[\kappa_2 (f + \kappa_2)^2 - \kappa_3 (f + \kappa_3)^2 \right] \sinh \kappa_c - \kappa_c [\kappa_2 (f + \kappa_2) - \kappa_3 (f + \kappa_3)] \cosh \kappa_c}{(\kappa_2 - \kappa_3) (G_2 \cosh \kappa_c - G_1 \sinh \kappa_c)}. \end{aligned} \quad (42)$$

We are interested in deriving an expression for the pressure Π in the limit $f \rightarrow \infty$, *i.e.*, in the case in which the particle is confined in a box ($x \in [-1 : 1]$). From Eq. (36) for large f we have

$$\kappa_1 = 2\Gamma \frac{L^2}{R^2} \frac{1}{f} + O\left(\frac{1}{f^2}\right), \quad (43a)$$

$$\kappa_2 = -f + \frac{L}{R} \text{Pe} - \frac{L^2}{R^2} \Gamma \frac{1}{f} + O\left(\frac{1}{f^2}\right), \quad (43b)$$

$$\kappa_3 = -f - \frac{L}{R} \text{Pe} - \frac{L^2}{R^2} \Gamma \frac{1}{f} + O\left(\frac{1}{f^2}\right). \quad (43c)$$

Using the above asymptotic expansion, after some algebra we get

$$G_1 = -\text{Pe}^2 \frac{L^2}{R^2} f^2 + O(f), \quad G_2 = 2\Gamma \frac{L^2}{R^2} \kappa_c f^2 + O(f), \quad (44a)$$

$$A_c = \bar{\rho} \frac{\kappa_c \text{Pe}^2}{\text{Pe}^2 \sinh \kappa_c + 2\Gamma \kappa_c \cosh \kappa_c} + O\left(\frac{1}{f}\right), \quad B_c = \bar{\rho} \frac{2\Gamma \kappa_c \cosh \kappa_c}{\text{Pe}^2 \sinh \kappa_c + 2\Gamma \kappa_c \cosh \kappa_c} + O\left(\frac{1}{f}\right). \quad (44b)$$

Finally, from Eq. (42) we get

$$\Pi = \bar{\rho} \frac{R^2}{L^2} \frac{\kappa_c^3 \cosh \kappa_c}{\text{Pe}^2 \sinh \kappa_c + 2\Gamma \kappa_c \cosh \kappa_c} - \frac{1}{f} \bar{\rho} \frac{R^2}{L^2} \frac{\kappa_c^4 (\text{Pe}^2 + 2\Gamma \cosh^2 \kappa_c)}{(\text{Pe}^2 \sinh \kappa_c + 2\Gamma \kappa_c \cosh \kappa_c)^2} + O\left(\frac{1}{f^2}\right), \quad (45)$$

therefore

$$\Pi_\infty = \lim_{f \rightarrow \infty} \Pi = \bar{\rho} \frac{R^2}{L^2} \frac{\kappa_c^3 \cosh \kappa_c}{\text{Pe}^2 \sinh \kappa_c + 2\Gamma \kappa_c \cosh \kappa_c}. \quad (46)$$

From Eqs. (33) and (41) for $-1 \leq x \leq 1$

$$\rho_\infty(x) = \lim_{f \rightarrow \infty} \rho(x) = \kappa_c \bar{\rho} \frac{\text{Pe}^2 \cosh(\kappa_c x) + 2\Gamma \cosh \kappa_c}{\text{Pe}^2 \sinh \kappa_c + 2\Gamma \kappa_c \cosh \kappa_c}, \quad (47a)$$

$$\delta \rho_\infty(x) = \lim_{f \rightarrow \infty} \delta \rho(x) = \kappa_c^2 \bar{\rho} \frac{R}{L} \frac{\text{Pe} \sinh(\kappa_c x)}{\text{Pe}^2 \sinh \kappa_c + 2\Gamma \kappa_c \cosh \kappa_c}. \quad (47b)$$

For $|x| > 1$ we get $\rho_\infty(x) = \delta \rho_\infty(x) = 0$.

Comparison with Nat. Phys. 11, 673(2015)

In order to compare with the results of Nat. Phys. 11, 673(2015) (Ref. [34] of the main text) we calculate

$$\frac{\Pi_\infty}{\rho_\infty(x=0)} = \frac{(\text{Pe}^2 + 2\Gamma) \cosh(\kappa_c)}{\text{Pe}^2 + 2\Gamma \cosh(\kappa_c)}, \quad (48)$$

which for $\kappa_c \gg 1$ reduces to

$$\frac{\Pi_\infty}{\rho_\infty(x=0)} = \frac{\text{Pe}^2}{2\Gamma} + 1, \quad (49)$$

the result reported in Ref. [34]. Note that $\kappa_c = \frac{L}{R} \sqrt{\text{Pe}^2 + 2\Gamma} \gg 1$ can be attained for systems whose size is

$$L \gg \frac{R}{\sqrt{\text{Pe}^2 + 2\Gamma}} \quad (50)$$

The discrepancy between our formula (Eq. (6) of the main text) and Nat. Phys. 11, 673(2015) (Ref. [34] of the main text) is relevant for weakly active systems, *i.e.*, for $\text{Pe} \lesssim 1$ and $\Gamma \lesssim 1$. We note that, thanks to our approach, we can compute the full value of Π_∞ on the top of its “deviation” from the ideal gas law, $\Pi_\infty/\rho_\infty(x=0)$.

Numerical simulations

We perform Brownian dynamics simulations of ABPs confined between two infinite parallel plates kept at distance L . In order to mimic infinite walls, periodic boundary conditions are applied on the top and bottom wall (*i.e.*, along the y axis) whereas particles cannot cross the walls on the x axis. When a particle attempts to cross the wall, its position is reset to the previous one and it interchanges a momentum

$$\Delta p = 2mv_{\perp}. \quad (51)$$

where v_{\perp} is the component of the velocity perpendicular to the wall. Pressure is calculated by summing all these momentum changes per unit time over a time step and then averaged over the simulation time.

Compressibility

Here we derive the expression for the compressibility

$$H_{\infty} = -\frac{1}{L} \left(\frac{\partial \Pi_{\infty}}{\partial L} \right)^{-1} = \left(\frac{L}{R} \right)^3 \frac{4 (\text{Pe}^2 \sinh \kappa_c + 2\Gamma \kappa_c \cosh \kappa_c)^2}{\kappa_c^4 (2\Gamma \cosh \kappa_c + \text{Pe}^2)} = \frac{1}{\Pi_{\infty}} \frac{(2\Gamma \kappa_c \cosh \kappa_c + \text{Pe}^2 \sinh \kappa_c) \cosh \kappa_c}{\kappa_c (\text{Pe}^2 + 2\Gamma \cosh^2 \kappa_c)}. \quad (52)$$

Notice that in the limit $\kappa_c \gg 1$ the last expression reduces to

$$H_{\infty} = \frac{1}{\Pi_{\infty}} \frac{2\Gamma \kappa_c + \text{Pe}^2}{2\Gamma \kappa_c}. \quad (53)$$